Journal of Marine Science and Application (2026) 25: 1196-1212
https://doi.org/10.1007/s11804-026-00861-2

RESEARCH ARTICLE

CFD-Based Hydrodynamic Optimization of Inland Ships

S M Rashidul Hasan[1], and Md. Mashud Karim[2]

Received: 04 May 2025 / Accepted: 20 October 2025
© Harbin Engineering University and Springer-Verlag GmbH Germany, part of Springer Nature 2026

Abstract

This study validates a set of proposed design improvement methods for inland oil tankers and passenger ships in Bangladesh's inland waterways. Hydrodynamic performance is assessed using computational fluid dynamics (CFD) simulations. Three-dimensional models of three oil tankers and three passenger ships are created after physical investigations and measurements. These are reconfigured according to previously suggested qualitative and quantitative design recommendations. The CFD analysis results indicate very significant reductions in overall resistance for all the redesigned vessels, ranging from 5.56% to 17.27% for oil tankers and up to 16.97% for passenger ships. These reductions validate the effectiveness of the proposed design methods in improving energy efficiency. Although limitations due to operations are present with some of these recommendations, the overall performance improvements provide valuable insights for enhancing the designs of inland ships. However, to validate such computational findings and expand design processes, model testing of new designs is recommended.

Keywords Greenhouse gas; International maritime organization; Energy-efficiency design index; CO_2 emission; Inland ship

1 Introduction

Inland water transportation is a cornerstone of Bangladesh's economy, facilitating the movement of passengers and freight across an extensive network of rivers and canals. According to the Bangladesh Inland Water Transport Authority (BIWTA, 2023), this sector plays a crucial role in supporting national economic activities but faces challenges in achieving efficient and sustainable vessel designs (Natalia et al., 2024). Unlike ocean-going vessels, which are governed by standardized international design protocols, inland ships operate in diverse and often constrained environments, lacking universal design guidelines. Uddin et al. (2017) highlighted the absence of standardized frameworks for inland vessels, whereas Hasan and Karim (2020) emphasized the hydrodynamic challenges posed by shallow and confined waterways in Bangladesh, such as variable water depths and restricted channels.

Computational fluid dynamics (CFD) has become a vital tool for optimizing ship designs to address the aforementioned challenges. Previously, Onwuegbuchunam et al. (2019) demonstrated the efficacy of CFD in hull form optimization, achieving significant reductions in resistance for a supply vessel. Similarly, Du et al. (2020) explored the hydrodynamic performance of vessels in confined waterways. They used benchmark hull forms like the Kriso Container Ship and the Very Large Crude Carrier 2. Although these hull forms were associated with ocean-going vessels, their study provided a methodological foundation for analyzing resistance in restricted waterways, which is directly applicable to inland shipping. This inclusion of ocean-going vessel research served to contrast their established design standards with the variability of inland vessels and to adapt proven CFD techniques to the inland context, enhancing the robustness of their methodology.

Specifically for Bangladesh, Hasan and Karim (2020; 2022; 2023) advanced the field by proposing design optimizations for inland ships. Their works focused on reducing resistance and improving energy efficiency, tailored to the unique navigational conditions of Bangladesh's water-

Article Highlights

- In order for wave energy to be a viable energy option, the survivability in harsh offshore environments must be guaranteed.
- Peak forces in the connection line used in the wave energy concept developed at Uppsala University is studied.
- Three numerical models are presented and compared with each other and with physical wave tank data.
- The performance of each model is studied and seen dependent on buoy geometry and applied level of power take off damping.

✉ S M Rashidul Hasan
rashidul.naoe@bmu.edu.bd

[1] Department of Naval Architecture and Offshore Engineering, Bangladesh Maritime University, Mirpur-12, Dhaka-1216, Bangladesh

[2] Department of Naval Architecture and Marine Engineering, Bangladesh University of Engineering and Technology, Palashi, Dhaka-1000, Bangladesh

ways. For instance, Hasan and Karim (2020) proposed a revised Energy-Efficiency Design Index for inland oil tankers, addressing carbon dioxide (CO_2) emission reduction. Their subsequent studies (Hasan and Karim, 2022; 2023) further developed energy-efficient designs and CO_2 reduction strategies, emphasizing the need for context-specific solutions. However, these studies primarily focused on theoretical and preliminary designs, with limited empirical validation under real-world operating conditions.

Depending on the engine's age and condition, the specific fuel consumption (SFC) of ships typically ranges from 195 to 220 g/kWh (Rørdam et al., 2009). However, a recent study on Bangladeshi inland ships reported SFC values of 198 – 238 g/kWh, based on physical fuel measurements from 15 vessels operating at service speed (Hasan and Karim, 2022). On average, this indicates that the inland fleet in Bangladesh consumes ~10.5 g/kWh more fuel than standard benchmarks. As fuel consumption is directly correlated with greenhouse gas (GHG) emissions, this excess translates into a significantly higher carbon footprint, underscoring the need for design and propulsion system improvements in the country's inland water transport sector.

Sustainability is another critical aspect of inland water transportation. Rørdam et al. (2009) highlighted the environmental impact of shipping, emphasizing the need for energy-efficient designs to reduce fuel consumption and emissions. Meanwhile, Hasan and Karim (2022) echoed this, advocating for designs that minimize the carbon footprint of inland vessels. This study aligns with these goals by optimizing hull forms to reduce resistance, thereby lowering fuel consumption and emissions.

For sensitivity analysis, we employed the Holtrop–Mennen method (Holtrop and Mennen, 1982), originally developed for ocean-going vessels, to estimate hydrodynamic resistance and assess design parameters. Its application to inland ships demonstrates the adaptability of established methods to new contexts, providing a quick and reliable tool for preliminary design evaluations.

In this study, we adopt standard numerical analysis terminology to ensure clarity. Verification refers to confirming the numerical accuracy of CFD simulations, typically through grid-convergence studies and residual analysis, ensuring the computational model accurately solves mathematical equations (Dowding and Sandia National Laboratories, 2016). Validation involves assessing CFD results against established benchmarks and hydrodynamic performance metrics to assess their physical accuracy and ensure practical applicability (Orych et al., 2021). Although theoretical models and limited practical applications of ship design improvements have shown promise, comprehensive validation is still required to confirm their effectiveness in real-world conditions, particularly in Bangladesh's inland waterways. In practice, the validation of inland ship design improvement procedures in Bangladesh is not only a technical process but is also essential for enhancing efficiency and sustainability. Although studies like those of Hasan and Karim (2020; 2022; 2023) have proposed innovative designs, only a few have validated these models against experimental or operational data to confirm their effectiveness in real-world scenarios, such as navigating shallow and confined waterways. This study addresses this gap by using CFD simulations to validate and refine design optimizations for inland oil tankers and passenger ships, ensuring their practical applicability and effectiveness in Bangladesh's challenging navigational environment.

2 Methodology

To validate the ship design recommendations for Bangladesh's inland passenger ships and oil tankers proposed by Hasan and Karim (2022), an extensive analysis was conducted by following the methodology below. Validation was conducted by comparing CFD simulation results with hydrodynamic resistance data derived from ship hull line plans and model tests. These data were utilized as they provide insight into the differences in performance between original and redesigned hulls in actual operating conditions. The methodology followed in this study is discussed below.

2.1 Selection and physical measurement of hulls

The hulls of three oil tankers and three passenger ships operating in Bangladesh's inland waterways were selected for physical measurement. This step was essential because discrepancies between documented line plans and actual hull shapes were frequently observed for inland ships in Bangladesh. Accurate physical measurements were performed to capture the exact geometries of these vessels.

2.2 3D modeling of hulls

The measured hull geometries were converted into three-dimensional (3D) models using the ship design software Maxsurf. This conversion was necessary to ensure a precise digital representation of the existing hulls, which were then used as the baseline for further analysis.

2.3 Application of the proposed design recommendations

During hull remodeling, both qualitative and quantitative ship design principles were strictly followed. The process involved parametric transformations, where the principal particulars of the ships were either increased or decreased according to the proposed recommendations. Notably, the remodeled hulls were intentionally unfaired

to ensure that the transformation adhered strictly to the design recommendations.

2.4 Maintaining consistent parameters

To facilitate an equitable comparison between the existing and redesigned hulls, the remodeled versions were configured to have the same displacement and operational speed as the original hulls. This consistency ensured that any observed performance differences could be attributed solely to variations in hull design rather than other variables such as weight or speed.

2.5 Resistance analysis using CFD

Both the original and remodeled hulls were tested using the CFD software Shipflow. Resistance analysis was conducted on each model, with particular emphasis on hydrodynamic resistance and its corresponding coefficients. Comparing the resistance values of the existing and redesigned hulls enabled the assessment of the impact of the proposed design modifications on the overall performance of the vessels.

The choice of Shipflow as the CFD platform was due to its zonal solver structure, speed, and proven accuracy in predicting resistance for ship hull forms in preliminary design stages. Although general-purpose CFD platforms like Star-CCM+ and OpenFOAM offer higher-fidelity Reynolds-averaged Navier–Stokes (RANS) solvers, they require significantly more computational time. Shipflow was selected for its balance of computational efficiency and accuracy, which are particularly suited to the needs of this multiship comparative study. Future work may consider full-RANS-based simulations using OpenFOAM or Star-CCM+ to enhance flow detail analysis.

2.6 Comparison of resistance coefficients

This study compared the resistance coefficients of the remodeled and original hulls. These coefficients served as the primary indicators for the measurement of the hydrodynamic efficiency of the redesigned vessels. The observed resistance variations provided the basis for assessing the efficiency of the recommended design proposals.

2.7 Limitations and assumptions

This study relied entirely on CFD simulations because of financial and logistical constraints, which prevented physical model testing. Although advanced CFD tools provide reliable insights into fluid–structure interactions and allow for efficient parametric analysis, they also introduce certain limitations.

First, the simulations assumed incompressible, turbulent flow and idealized boundary conditions, which might not fully capture real-world complexities, such as turbulence modeling errors and boundary-layer effects. Although both original and redesigned hulls were analyzed under identical conditions to ensure fair comparison, caution was warranted when interpreting absolute values of resistance, particularly in the absence of experimental validation. Future studies should incorporate towing tank or full-scale trials to strengthen the accuracy of CFD-based conclusions.

In addition to methodological constraints, several scope-related limitations apply. All simulations were conducted under calm water conditions. This excluded wave, wind, or current influences, which commonly affect inland vessel performance. The optimization had a single objective, focusing solely on resistance reduction, without accounting for critical parameters such as stability and maneuverability. Furthermore, resistance was evaluated only at the design draft, omitting performance variations across ballast, part-load, or overloaded conditions—scenarios frequently encountered in practice.

These limitations define the boundaries of this study while guiding future research directions. To improve robustness, future work should adopt multiobjective optimization frameworks, incorporate environmental variability, and evaluate performance across a range of operating drafts to enhance the real-world applicability of hydrodynamic design improvements.

3 Theoretical background of the CFD solver for analyzing viscous flow

Statistical turbulence has been a subject of research since its first identification, with foundational contributions credited to Osborne Reynolds and, previously, implied references in Boussinesq's work (Boussinesq, 1878). Among the pioneers of this area were Reynolds, Prandtl (Prandtl, 1904), and Taylor, who emphasized the perceived randomness of turbulent flows and proposed that statistical methods were the only viable means of analysis (Cheng et al., 2017). This stance remained prevalent in the development stages of turbulence modeling, which was largely influenced by the averaging of the following nonlinear Navier–Stokes (N–S) equations:

$$\frac{\partial u}{\partial t} + u\frac{\partial u}{\partial x} + v\frac{\partial u}{\partial y} + w\frac{\partial u}{\partial z} = -\frac{1}{\rho}\frac{\partial p}{\partial x} + v\left(\frac{\partial^2 u}{\partial x^2} + \frac{\partial^2 u}{\partial y^2} + \frac{\partial^2 u}{\partial z^2}\right)$$

$$\frac{\partial v}{\partial t} + u\frac{\partial v}{\partial x} + v\frac{\partial v}{\partial y} + w\frac{\partial v}{\partial z} = -\frac{1}{\rho}\frac{\partial p}{\partial y} + v\left(\frac{\partial^2 v}{\partial x^2} + \frac{\partial^2 v}{\partial y^2} + \frac{\partial^2 v}{\partial z^2}\right)$$

$$\frac{\partial w}{\partial t} + u\frac{\partial w}{\partial x} + v\frac{\partial w}{\partial y} + w\frac{\partial w}{\partial z} = -\frac{1}{\rho}\frac{\partial p}{\partial z} + v\left(\frac{\partial^2 w}{\partial x^2} + \frac{\partial^2 w}{\partial y^2} + \frac{\partial^2 w}{\partial z^2}\right)$$

The N−S equations may be reduced to a form suitable for numerical solutions, with the help of advancements in computational power at present. This entails breaking down pressure and velocities into their fluctuating and time-averaged portions. This is called the RANS method. The time-averaged velocities are labeled as $u_i = \bar{u}_1 + u_i'$, where $\bar{u}_1$ is the average and u_i' is the fluctuating component in the x-, y-, and z-directions. By time-averaging the N–S equations, all turbulent fluctuations essentially disappear, apart from the Reynolds stresses. These stresses add six further unknowns to a situation already involving four equations. The solution to this problem is obtained by correlating the Reynolds stresses with the average velocities using a turbulence model in combination with RANS (Eliasson and Olsson, 2011).

The RANS solver utilizes the finite volume technique, which divides the numerical space into many small discrete cells. The governing relations are summed over each cell before the variable of concern is determined using the cell centroid value. Because the boundary errors between adjacent cells cancel out, the finite volume technique enforces the conservation of basic quantities, such as mass, momentum, and energy.

The increased processing power of computers today has opened many windows for solving numerical problems. CFD solves and analyzes viscous and inviscid fluid flow problems using data structures and numerical analysis. By providing an initial design evaluation at relatively low cost, CFD can substitute for physical experiments, at least for typical hull shape types.

The simulation process using CFD starts with the development of a mathematical model that represents the ship's hull geometry (Larsson and Hoyte, 2010). After physical issues are recognized, a conceptual mathematical model is developed. This includes several sets of differential or integral equations. First, these equations must be discretized to offer numerical solutions (Nabila, 2014). Next, numerical methods are utilized to obtain solutions. At each step, however, some level of inaccuracy is introduced to the resulting solution (Nabila, 2014). These errors come from assumptions in the development of the conceptual model, as well as from approximations in the equations, such as linearization and the addition of empirical information.

The shear−stress transport (SST) $k-\omega$ model is used because of its ability to accurately capture boundary-layer separation and provide high accuracy near walls.

This model effectively blends k–ε behavior in free-stream flow with the k–ω behavior near walls.

The transport equations for turbulent kinetic energy (k) and specific dissipation rate (ω) in the SST k–ω model are as follows:

$$\frac{\partial k}{\partial t} + \frac{\partial\left(u_j k\right)}{\partial x_j} = -\overline{u_i'' u_j''}\frac{\partial u_i}{\partial x_j} - \beta^* k\omega + \frac{\partial}{\partial x_j}\left(\left(v + \sigma_k v_T\right)\frac{\partial k}{\partial x_j}\right)$$

$$\frac{\partial \omega}{\partial t} + \frac{\partial\left(u_j \omega\right)}{\partial x_j} = -\frac{\gamma}{v_T}\overline{u_i'' u_j''}\frac{\partial u_i}{\partial x_j} - \beta^* \omega^2 + \frac{\partial}{\partial x_j}\left(\left(v + \sigma_\omega v_T\right)\frac{\partial \omega}{\partial x_j}\right) + 2\sigma_{\omega 2}\frac{1 - F_1}{\omega}\frac{\partial k}{\partial x_j}\frac{\partial \omega}{\partial x_j}$$

"XCHAP" is the finite volume code of FLOWTECH International AB, Sweden (Eliasson and Olsson 2011). It serves as the RANS equation solver integrated within the Shipflow software. It incorporates several turbulence models (e. g., explicit algebraic stress model (EASM), $k-\omega$ baseline (BSL), and k–ω SST). The solver can operate in zonal or global modes and includes parameterized appendage models for components such as rudder, shafts, brackets, and vortex generators. It also supports grid files generated from standalone grid generator programs. Its simple force model and lifting line model can be used as actuator disk models. Shipflow (used herein), which utilizes XCHAP, can compute the following values:

i. Velocity field

ii. Pressure

iii. Turbulent kinetic energy and specific turbulent kinetic energy

iv. Local skin friction coefficient

v. Friction and pressure resistance coefficients for the grid-covered portion of the hull

vi. Total resistance and its components.

CFD analysis fulfills both Froude and Reynolds similarities, which is its main benefit. That is, results at the model and full scales are available directly while providing information on the flow.

3.1 CFD solver

The CFD simulations in this study were conducted using 'Shipflow' software which employs a zonal approach (Eliasson and Olsson, 2011) to model the flow around inland ship hulls. The flow field was divided into three nonoverlapping zones (Figure 1) to balance accuracy and computational efficiency. Zone 1 used XPAN, a nonlinear Rankine-panel potential flow solver, to compute wave resistance across the entire hull. Zone 2 used XBOUND to calculate boundary-layer effects. Zone 3 used XCHAP, a RANS solver, to compute viscous flow in the aft region. XPAN generated a free-surface database file (id_XPDB), which XBOUND and XCHAP used to incorporate wave and boundary-layer effects into viscous flow calculations. The total resistance was obtained by summing wave resistance (from XPAN), frictional resistance (from XBOUND), and

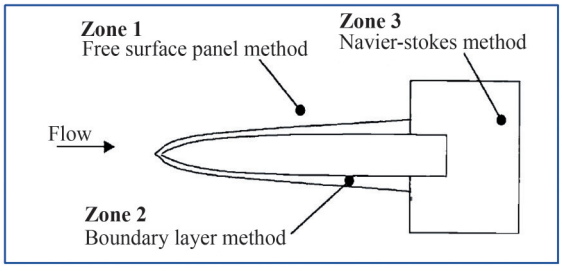


Figure 1 Zonal approach (Eliasson and Olsson, 2011)

viscous pressure resistance (from XCHAP).

The simulations were steady state with the ship fixed (0 degrees of freedom for rigid-body motion) and ran at a model scale (1 : 1) for Froude numbers in the range of 0.15–0.30, which matches typical inland ship speeds in Bangladesh. The XMESH module generated the surface panel mesh for XPAN (in the order of 10^4 panels), whereas the viscous zone (XCHAP) used a structured hexahedral volume mesh (in the order of 10^6 cells in medium refinement). We conducted a grid-convergence study with coarse/medium/fine meshes. The medium mesh (used for final runs) was within ~3% of the extrapolated solution. A representative panel–mesh illustration (Figure 1) shows the panel distribution used on a sample hull.

In Shipflow's hybrid scheme, XPAN (potential flow) and XCHAP (RANS) are coupled via an intermediate database. Specifically, XPAN computes the nonlinear free-surface solution and outputs a database file (id_XPDB). XBOUND and XCHAP then import these data to incorporate wave effects and boundary-layer calculations. Thus, the wave profiles and contours from XPAN's solution, seamlessly combined with the XCHAP flow field using the zonal approach (Eliasson and Olsson, 2011).

3.2 Mesh generation, boundary condition, and physics modeling

In this study, the functionalities of XMESH, XPAN, XBOUND, XGRID, and XCHAP within the Shipflow framework were used to simulate the resistance characteristics of inland vessels. The XMESH module generated the panel mesh required for the XPAN potential flow solver. XPAN outputs a database file (id_XPDB), which serves as a central input to XBOUND, XGRID, and XCHAP for further viscous flow and resistance analyses using the zonal approach.

To minimize boundary-induced inaccuracies, the computational domain was sized following established practices in naval CFD studies. The domain extended $3L$ upstream, $6L$ downstream, $2L$ laterally (both port and starboard), $2L$ above the free surface, and $1.5T$ below the keel, where L is the waterline length and T is the draft of the ship. These settings ensured adequate space for wave development and reduced boundary reflection. Symmetry was not applied as the simulations included full free-surface effects. The computational domain was discretized with structured hexahedral meshes, with local refinement near the hull surface and the free surface to accurately resolve boundary-layer behavior and wave patterns.

Figure 2 illustrates the boundary conditions used for the flow domain (Bappy and Hasan, 2024). The green-colored surface denotes the outflow boundary, with inflow at the opposite side. A no-slip condition was applied on the hull surface (zero velocity), whereas the remaining domain boundaries used slip conditions. These boundary conditions, along with the zonal solution methodology, allowed the efficient resolution of both viscous and inviscid regions of the flow.

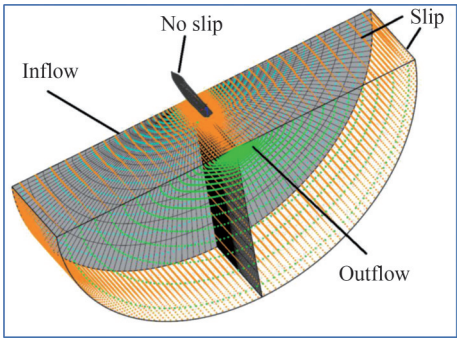


Figure 2 Boundary conditions for the hull (Bappy and Hasan, 2024)

XBOUND handled the boundary-layer calculations and passed data to XCHAP, which solved the RANS equations using the finite volume method. Among various turbulence models (EASM, k–ω BSL, and k–ω SST), the SST k–ω model was used because of its superior performance near the wall and in regions of adverse pressure gradients. The turbulence intensity was set to 5%, and standard wall function treatments were applied. Free-surface effects were modeled using XPAN's panel-based potential flow solver, coupled with viscous correction in XCHAP. The total resistance was computed by combining the contributions from XPAN (wave resistance), XBOUND (boundary layer), and XCHAP (viscous pressure effects).

The XPAN free-surface solver in Shipflow has been benchmarked extensively against International Towing Tank Conference standard cases and experimental towing tank data for slender hulls at Froude numbers ranging from 0.15 to 0.30. In these studies, XPAN consistently achieved a mean free-surface elevation accuracy within ±5 mm. Given that the Froude numbers in this study fall within this validated range (F_N = 0.17–0.26), the wave patterns computed here can be considered physically reliable.

3.3 Verification and validation

Unsteady Shipflow simulations were conducted using the software's hybrid potential/RANS approach, where the XPAN and XCHAP solvers were combined (Orych et al.,

2021). In XCHAP, we employed EASM with no wall functions and full boundary-layer resolution in a double-model formulation. This ensured that viscous and wave-resistance components were both captured accurately. The solver was run in transient mode: each time step was iterated until residuals dropped by several orders of magnitude (typically from 10^{-5} to 10^{-6}), well beyond the ASME V&V recommendation that iteration errors be much smaller than the discretization error. In practice, we monitored momentum and continuity residuals at each step, confirming that they fell by at least 3–4 decades from initialization before advancing the solution. The chosen time step (usually 0.02 – 0.05 s) gave Courant numbers of $\lesssim 1$ for the flow velocities, which reduced the time step further and had a negligible effect on the resistance time series, indicating adequate temporal discretization (Courant et al., 1967).

A systematic grid-refinement study was performed using three meshes. All meshes had the same domain dimensions and refined wall-normal spacing to maintain consistent boundary-layer resolution. Each mesh was run to quasisteady periodic behavior, and the time-averaged total resistance (averaged over several seconds after the initial transient) was recorded. The coarse, medium, and fine meshes yielded average nondimensional $C_T = 4.06 \times 10^{-3}$, 3.86×10^{-3}, and 3.74×10^{-3}, respectively. The application of Richardson extrapolation and the grid-convergence index (GCI) procedure (Celik et al., 2007) to these three results gave a fine – medium GCI of about 3%. This confirmed that the medium mesh was within ~3% of the converged solution. In accordance with best practices, the apparent convergence order was checked and found to be near the expected second-order, indicating that the meshes were in the asymptotic range. Because the GCI was well below 5%, the medium mesh was adopted for all subsequent cases, balancing accuracy and computational cost.

Each unsteady run was allowed to reach a periodic steady state before the statistics were sampled. Typically, the flow fields and forces stabilized (oscillating about a mean) after 2–3 s of physical time. Figure 3 shows a sample force (total resistance) history for the medium mesh case. After initial transients, the force oscillated about a steady mean value, reflecting the unsteady wave–body interactions. In our analysis, the mean resistance was computed by averaging the force over a steady oscillation cycle. The residuals at each time step were driven down to ~10^{-5} for all equations. Additional iterations produced only a negligible force change (the iteration error was kept at least an order smaller than the GCI uncertainty). Thus, both spatial and temporal convergence criteria were satisfied.

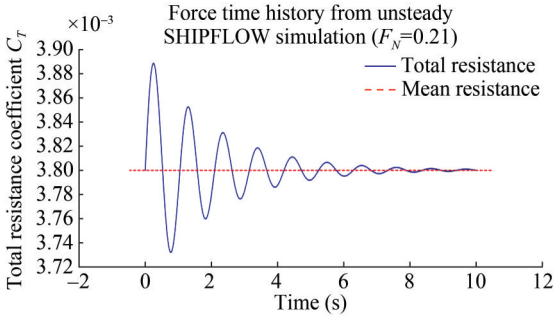


Figure 3 Sample time history of total resistance (N) from an unsteady Shipflow simulation

The curve in Figure 3 shows the force response over time for the medium mesh case at $F_N \approx 0.21$. After an initial transient ($t \approx 0-2$ s), the solution reached a periodic oscillation. The plotted data were used to compute the steady mean resistance (horizontal dashed line) for V&V analysis.

4 Calculations and results

The redesign of existing ship hulls was based on the following qualitative and quantitative guidelines, as proposed by the authors. Tables 1 and 2 summarize the energy-efficient ship design parameters found after analyzing 134 oil tankers and 479 passenger ships of Bangladesh. This analysis was previously done by the authors (Hasan and Karim, 2022).

Table 1 Proposed efficient ship design ranges for oil tankers in Bangladesh

L_{WL} (m)	L_{WL}/B	B/T	DWT/∇	V_s (kn)	F_N	C_B
$L_{WL} < 51$	4.23–6.13	1.90–5.00	0.72–0.83	8.00–10.50	0.19–0.24	Lowest possible C_B that meets capacity and stability requirements
$L_{WL} = 51–60$	5.20–7.15	1.86–3.24	0.65–0.83	8.00–10.50	0.17–0.23	
$L_{WL} > 60$	5.33–6.73	2.38–3.28	0.66–0.80	8.00–11.00	0.16–0.21	

Table 2 Proposed efficient ship design ranges for passenger ships in Bangladesh

L_{WL} (m)	L_{WL}/B	B/T	GT	V_s (kn)	F_N	C_B
$L_{WL} < 31$	3.72–5.71	2.58–7.87	66–180	7.50–11.00	0.22–0.32	Lowest possible C_B that meets capacity and stability requirements
$L_{WL} = 32–45$	3.74–6.21	3.33–6.54	237–640	9.00–12.00	0.23–0.32	
$L_{WL} > 46$	5.01–6.39	3.39–8.47	681–3 704	10.00–14.00	0.21–0.27	

The design quality of these energy-efficient ships followed certain identifiable trends. These trends have been analyzed and explained using hydrodynamic theories within the field of naval architecture. Thus, a set of qualitative ship design recommendations has been developed, as presented in Table 3 which is. It is important to emphasize that, regardless of any modifications made to the new designs, they must fully comply with all mandatory stability criteria for these vessels.

Notably, ship design parameters are interdependent. For example, our target vessel's required displacement is 1 000 t. Because $L_{WL} \times B \times T \times C_B$ = Displacement, it is not difficult to predict a combination of principal particulars that will produce 1 000 when multiplied is not difficult. However, these parameters are interdependent and closely related to ship resistance.

Table 4 shows the aforementioned interdependence and why a holistic approach to ship design, particularly selection, is necessary. This example does not correspond to any of the six measured ships but is a conceptual case designed to isolate the effect of principal parameter changes. A sensitivity analysis for this sample ship isolated individual parameter effects. Resistance was calculated using the Holtrop–Mennen method, a regression-based calculation process derived from existing ship model test data (Holtrop and Mennen, 1982). This method is widely used for quick resistance estimation in preliminary design stages. Although it was primarily developed for sea-going vessels and might not accurately predict resistance for inland ships in shallow-water conditions, it was used here to illustrate the general sensitivity of total resistance to changes in key design parameters. This provides qualitative insights complementing the detailed CFD simulations conducted for specific inland ship designs, accounting for the unique hydrodynamic conditions of inland waterways.

The first row of Table 4 presents the parent hull particulars. The remaining three rows present the effects of changing one parameter on the other parameters, keeping the same displacement of the ship. For instance, only increas-

Table 3 Ship design recommendations based on sensitivity analysis (qualitative) (Hasan and Karim, 2020)

Ship design particulars	Ship design improvement recommendation	Hydrodynamic impact
L_{WL}	The length of the vessel should be the maximum possible that meets the required displacement and surface area.	a. The waterline length of a ship has a primary hydrodynamic influence on its resistance, hull volume, and sea keeping. b. The Reynolds number and the frictional resistance coefficient increase with the increase in length. c. Wave resistance decreases.
L_{WL}/B	Increasing the L/B ratio is recommended. However, all types of stability criteria must be fulfilled.	A higher L/B ratio ensures a slender and sharp hull, which provides better performance in waves by reducing wave resistance.
B/T	Decreasing the B/T ratio is recommended. This should be done by lowering the breadth and/or increasing the draft. As inland ships face draft restrictions, the maximum achievable draft should be used to achieve the required displacement.	a. The beam–draft ratio correlates strongly with residuary resistance, which increases for large B/T. b. The decrease in the B/T ratio due to the decrease in the breadth also increases the L_{WL}/B ratio. As discussed before, having a higher L_{WL}/B ratio is desirable to reduce wave resistance. Increasing the draft lowers the B/T ratio and allows for a larger propeller. c. For cases with a high B/T ratio, the propeller slipstream area is small concerning the midship section, which reduces propulsion efficiency. The waterline entrance angles increase in comparison with other ships with the same fineness. This leads to relatively high resistance.
DWT/∇	A high DWT/∇ is desirable.	This can be achieved by decreasing the lightship weight. A lighter ship faces lower hydrodynamic forces.
C_B	A minimum C_B is recommended to achieve the desired displacement.	A reduction in C_B slightly increases the hull steel weight. However, lowering the C_B lowers the required propulsion power, engine plant weight, and fuel consumption.
V_s and F_N	Lowering V_s and F_N is recommended.	a. By optimizing the surface area for a given ship volume, viscous resistance can be achieved. For a given speed, increasing the length of a ship and lowering the beam reduces the surface area and viscous resistance coefficient. b. As the ship speed increases, the waves generated by the ship and the energy required to generate these waves rise with it. This wasted energy or wave-making resistance often becomes a limiting factor in a ship's speed. There are more wave crests on the side of the hull at low speeds; at high speeds, the wavelength lengthens.

Table 4 Sensitivity analysis example of a 1 000-t displacement ship for a fixed block coefficient of 0.741

Parent ship hull data	L_{WL} (m)	B (m)	L_{WL}/B	T (m)	B/T	Displacement (t)	Total resistance (kN)
Parent	50.00	9.00	5.56	3.00	3.00	1 000	32.56
5% L_{WL} increased	52.50	8.5	6.17 (+11.08%)	3.024	2.81 (−6.33%)	1 000	31.77 (−2.43%)
5% B increased	48.80	9.45	5.16 (−7.19%)	2.93	3.23 (+7.67%)	1 000	33.32 (+2.33%)
5% T increased	48.80	8.78	5.56 (0%)	3.15	2.79 (−7%)	1 000	32.70 (+0.43%)

ing 5% of the waterline length of the ship increases the ship's displacement. Therefore, other parameters must be adjusted. For this reason, the beam and draft decrease, with an overall decrease in resistance of 2.43%. This change also supports the qualitative recommendations in Table 3, which suggested increasing the L_{WL}/B ratio and decreasing the B/T ratio.

The third row of Table 4 shows the effect of a 5% increase in the ship's beam. This is against the qualitative recommendation, which recommends a decrease in L_{WL}/B and an increase in B/T. The total resistance increases as well.

Table 4 was constructed for a constant C_B to isolate the effect of one parameter on the others. Because C_B = Displacement/($L_{WL} \times B \times T$), the effect of a change in one parameter can easily be compensated by changing C_B. In addition, as C_B is the coefficient of fineness, the streamline shape of the ship changes, which goes against the fair comparison between the parent and improved hulls (with results shown in later sections).

The dead weight to displacement ratios (gross tonnage (GT) for passenger ships) were kept fixed for both the parent and improved hulls. This is required for fair comparison because when two ships' resistances are compared, both have to be under the same operating conditions, like carrying the same amount of dead weight and having the same speed. Both the dead weight to displacement ratio and speed have a very high impact on ship resistance. Later sections show that, even when these two parameters were kept constant for both parent and improved hulls, resistance decreased for the improved hull using the ship design recommendations. However, as presented in Table 3, when a new ship must be designed, the recommendation is to increase the dead weight to displacement ratio and decrease the speed. Achieving these decreases the overall resistance even more.

4.1 Validation of the ship design recommendations

As discussed in Section 2, three oil tankers and three passenger ships (a total of six) that ply within the inland water of Bangladesh were investigated. Their hull shapes and sizes were measured physically, and line plans were developed. The principal particulars of these vessels are presented in Table 5.

4.2 Implementation of the design recommendations

The measured ship hulls presented in Table 4 were improved using the recommendations presented in Tables 1–3. Notably, only the principal particulars were updated. Moreover, for fair comparison, the ship speed and dead weight (GT for passenger ships) were kept the same for both parent and improved hulls.

Table 6 represents the investigated design parameters of an oil tanker named OT-1049. After implementing the ship design recommendations, the improved design parameters are presented, with the changes shown in percentages. All the qualitative and quantitative ship design improvement criteria were satisfied in the improved design.

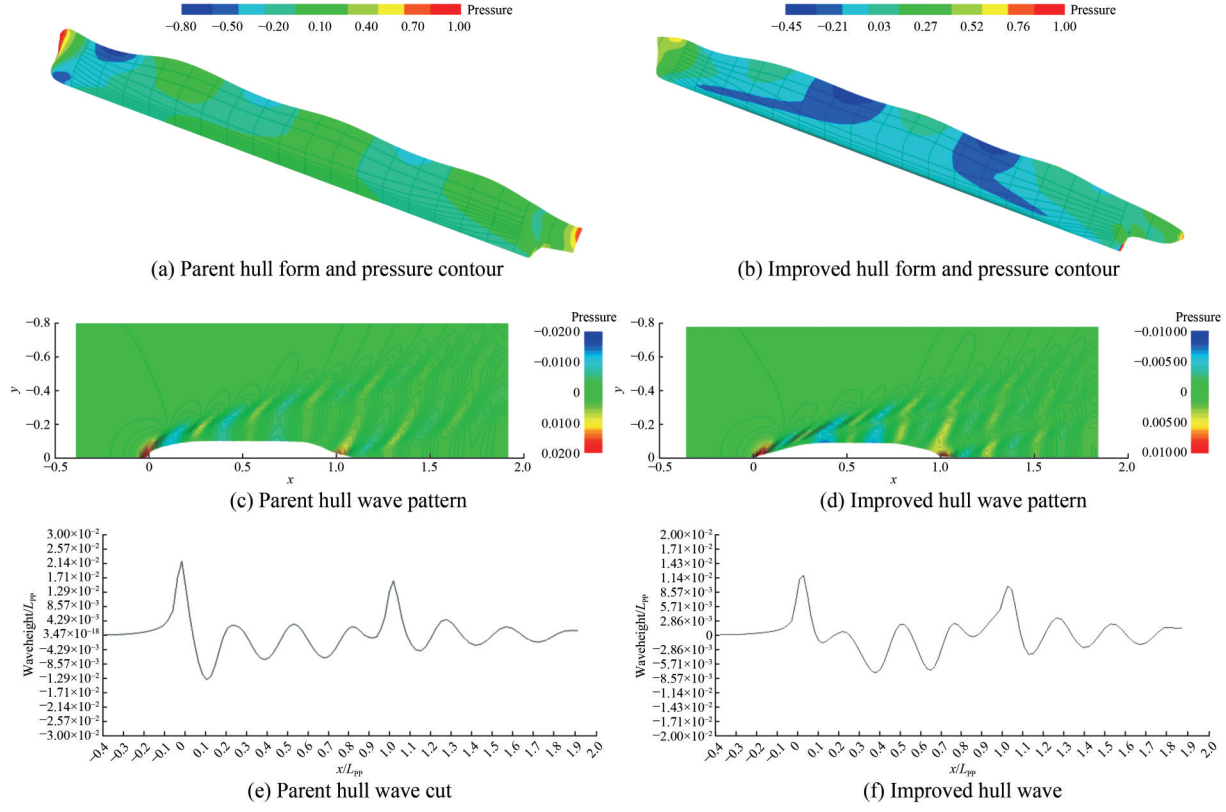
Figure 4 presents the wave patterns and wave cut for both the parent and improved hulls in the case of OT-1049. The improvements could be seen in the figure. Still, to facilitate better understanding, Table 6 is created. This table shows the actual changes in different resistance components. The total resistance was decreased by 7.95% (Table 7).

Table 5 Investigated vessels for validation

Principal particulars	Oil tanker			Passenger ship		
	OT 1049	OT zarifa	OT moina	MV running sun	MV ferry boat-1	MV Swapan
L_{WL}	49.73	53	73.77	34.15	47.97	43.76
B	10.13	11	12.45	6.77	10.62	7.77
T	3.04	1.8	4	1.35	2.25	1.6
∇	1 102	802	2 755	202	688	359
DWT (GT for passenger ships)	862	550	1 930	209	894	535
Main engine power (kW)	400 × 1	448 × 1	450 × 2	165 × 1	410 × 2	260 × 1
V_s	9	9	9	8	11	9.5

Table 6 Comparison between the parent and improved designs of OT-1049

Design particulars	Parent design	Improved design	Change (%)	Qualitative recommendation	Quantitative recommendation ranges	Design recommendations addressed?
L_{WL}	49.73	55	9.58	Increase	–	Yes
B	10.13	10	−1.30	–	–	–
L_{WL}/B	4.91	5.5	10.73	Increase	5.20–7.15	Yes
T	3.04	3.34	8.98	–	–	–
B/T	3.33	3	−11.00	Decrease	1.86–3.24	Qualitative recommendation addressed, but the adopted value is 2.77% higher than the upper limit of the quantitative range to obtain the same displacement for both hulls.
C_B	0.72	0.6	−20.00	Minimum C_B that meets capacity and stability requirements		Yes
F_N	0.21	0.2	−5.00	Decrease	0.17–0.23	Yes
DWT/∇	0.78	0.78	0.0	Increase	0.65–0.83	For fair comparison, this ratio was kept the same for both cases. Therefore, the qualitative recommendation was not met.
V_s	9	9	0.0	Decrease	8.00–10.50	For fair comparison, the speed was kept the same for both cases. Therefore, the qualitative recommendation was not met.



(a) Parent hull form and pressure contour

(b) Improved hull form and pressure contour

(c) Parent hull wave pattern

(d) Improved hull wave pattern

(e) Parent hull wave cut

(f) Improved hull wave

Figure 4 Wave pattern and wave cut of OT-1049

Table 7 Resistance coefficients for both parent and improved hulls of OT 1049

Resistance coefficient	Parent hull	Improved hull	Change (%)
C_F	1.68×10^{-3}	1.813×10^{-3}	8.05
C_{PV}	9.16×10^{-4}	7.79×10^{-4}	−14.93
C_V	2.594×10^{-3}	2.592×10^{-3}	−0.08
C_W	1.467×10^{-3}	1.146×10^{-3}	−21.88
C_T	4.061×10^{-3}	3.738×10^{-3}	−7.95

Similarly, the second and third inland oil tankers' data are presented (Tables 8, 9 and 10, 11). All the qualitative and quantitative design recommendations were satisfied as well in these cases.

Figure 5 presents the wave patterns and wave cut for both the parent and improved hulls in the case of OT Zarifa. The improvements are also presented numerically in Table 9. Overall, the improved design achieved a 17.27% reduction in resistance.

Table 8 Comparison between the parent and improved designs of OT Zarifa

Design particulars	Parent design	Improved design	Change (%)	Qualitative recommendation	Quantitative recommendation ranges	Design recommendations addressed?
L_{WL}	53	60	11.67	Increase	–	Yes
B	11	10	−10.00	–	–	–
L_{WL}/B	4.82	6	19.67	Increase	5.20–7.15	Yes
T	1.8	2.23	19.28	–	–	–
B/T	6.11	4.48	−26.67	Decrease	1.86–3.24	Qualitative recommendation addressed, but the adopted value is 38.27% higher than the upper limit of the quantitative range to obtain the same displacement for both hulls.
C_B	0.765	0.6	−27.50	Minimum C_B that meets capacity and stability requirements		Yes
F_N	0.2	0.19	−5.26	Decrease	0.17–0.23	Yes
DWT/∇	0.68	0.68	0.0	Increase	0.65–0.83	For fair comparison, this ratio was kept the same for both cases. Therefore, the qualitative recommendation was not met.
V_s	9	9	0.0	Decrease	8.00–10.50	For fair comparison, the speed was kept the same for both cases. Therefore, the qualitative recommendation was not met.

Table 9 Resistance coefficients for both the parent and improved hulls of OT Zarifa

Resistance coefficient	Parent hull	Improved hull	Change (%)
C_F	1.84×10^{-3}	1.71×10^{-3}	−7.06
C_{PV}	5.50×10^{-4}	6.50×10^{-3}	17.52
C_V	2.39×10^{-3}	2.36×10^{-3}	−1.42
C_W	1.64×10^{-3}	9.80×10^{-4}	−40.33
C_T	4.04×10^{-3}	3.34×10^{-3}	−17.27

In the case of OT Moina (Figure 6), the improved design achieved an overall 5.56% reduction in resistance (Table 11).

The analysis done for the oil tankers was also applied to three passenger ships. Table 12 presents the parent and improved hull design parameters for the passenger vessel named MV Ferry Boat-1. All qualitative and quantitative design recommendations were complied with.

Table 13 summarizes all the changes in the resistance components of MV Ferry Boat-1. A total of 11.82% reduction in resistance was achieved by the improved hull.

Figure 7 presents the wave patterns and wave cut for both the parent and improved hulls of MV Ferry Boat-1.

In the case of MV Sawapan (Table 14), the qualitative design recommendation could not be satisfied. This was primarily because this ship runs through a very limited water depth, where drafts over 1.82 m may cause grounding.

Although not all design recommendations could be followed for MV Swapan, a 12.98% decrease in total resistance could be achieved (Table 15).

Table 10 Comparison between the parent and improved design of OT Moina

Design particulars	Parent design	Improved design	Change (%)	Qualitative recommendation	Quantitative recommendation ranges	Design recommendations addressed?
L_{WL}	73.77	78	5.73	Increase	–	Yes
B	12.45	12	−3.61	–	–	–
L_{WL}/B	5.92	6.5	9.80	Increase	5.33–6.73	Yes
T	4	4	0	–	–	–
B/T	3.112	3	−3.60	Decrease	2.38–3.28	Yes
C_B	0.75	0.736	−1.87	Minimum C_B that meets capacity and stability requirements		Yes
F_N	0.172	0.1674	−2.67	Decrease	0.16–0.21	Yes
DWT/∇	0.7	0.70	0	Increase	0.66–0.80	For fair comparison, this ratio was kept the same for both cases. Therefore, the qualitative recommendation was not met.
V_s	9	9	0	Decrease	8.00–11.00	For fair comparison, the speed was kept the same for both cases. Therefore, the qualitative recommendation was not met.

Table 11 Resistance coefficients for both parent and improved hulls of OT Moina

Resistance coefficient	Parent hull	Improved hull	Change (%)
C_F	1.64×10^{-3}	1.61×10^{-3}	−1.83
C_{PV}	4.4×10^{-3}	3.6×10^{-4}	−19.10
C_V	2.08×10^{-3}	1.96×10^{-3}	−5.53
C_W	8.5×10^{-4}	8×10^{-4}	−5.60
C_T	2.93×10^{-3}	2.77×10^{-3}	−5.56

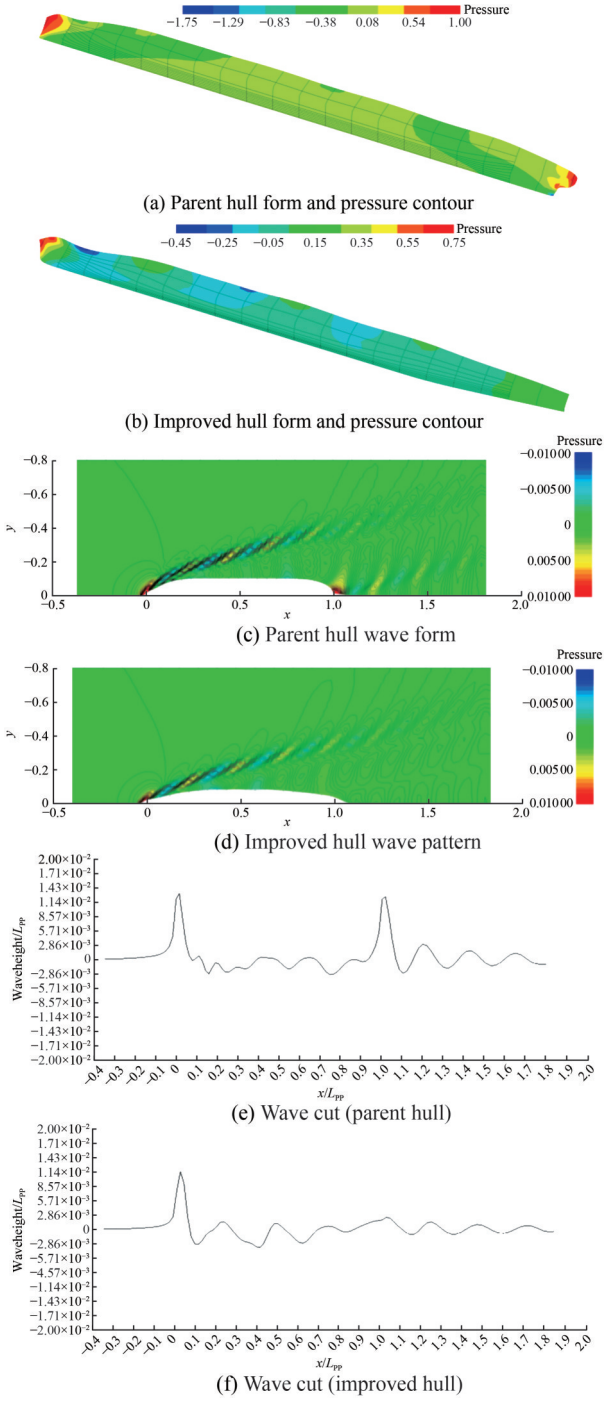


Figure 5 Wave pattern and wave cut of OT Zarifa

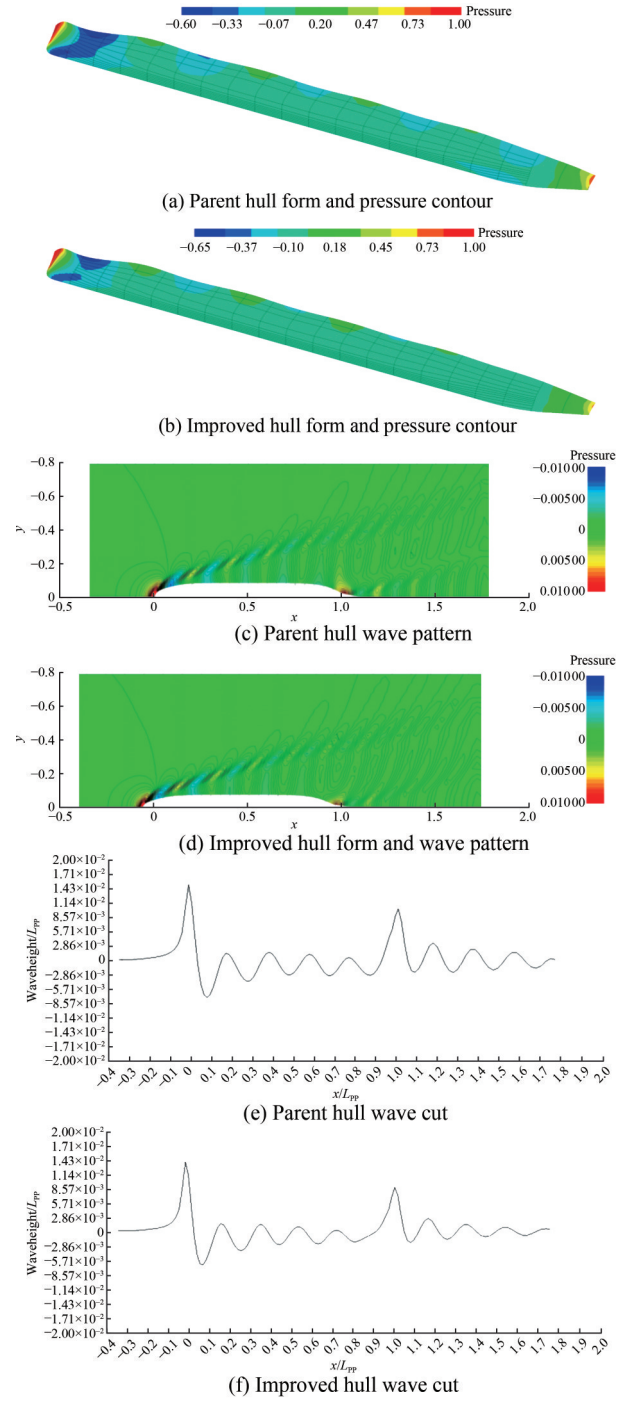


Figure 6 Wave pattern and wave cut of OT Moina

Figure 8 presents the wave patterns and wave cut for both the parent and improved hulls of MV Swapan.

Table 17 summarizes all the changes in the resistance components of MV Running Sun. A total of 16.97% reduction in resistance could be achieved by the improved hull.

Figure 9 presents the wave patterns and wave cut for both the parent and improved hulls of MV Running Sun.

All free-surface elevation plots (Figures 4–9) used a com-

Table 12 Comparison between the parent and improved designs of MV Ferry Boat-1

Design particulars	Parent design	Improved design	Change (%)	Qualitative recommendation	Quantitative recommendation ranges	Design recommendations addressed?
L_{WL}	47.97	52.10	8.61	Increase	–	Yes
B	10.62	9.10	−14.31	–	–	–
L_{WL}/B	4.52	5.73	26.77	Increase	5.01–6.39	Yes
T	2.25	2.20	−2.22	–	–	–
B/T	4.72	3.64	−22.88	Decrease	3.39–8.47	Yes
C_B	0.60	0.58	−3.33	Minimum C_B that meets capacity and stability requirements		Yes
F_N	0.26	0.25	−3.85	Decrease	0.21–0.27	Yes
GT	894	894	0	Increase	681–3 704	For fair comparison, GT was kept the same for both cases. Therefore, the qualitative recommendation was not met.
V_s	11	11	0	Decrease	10.00–14.00	For fair comparison, the speed was kept the same for both cases. Therefore, the qualitative recommendation was not met.

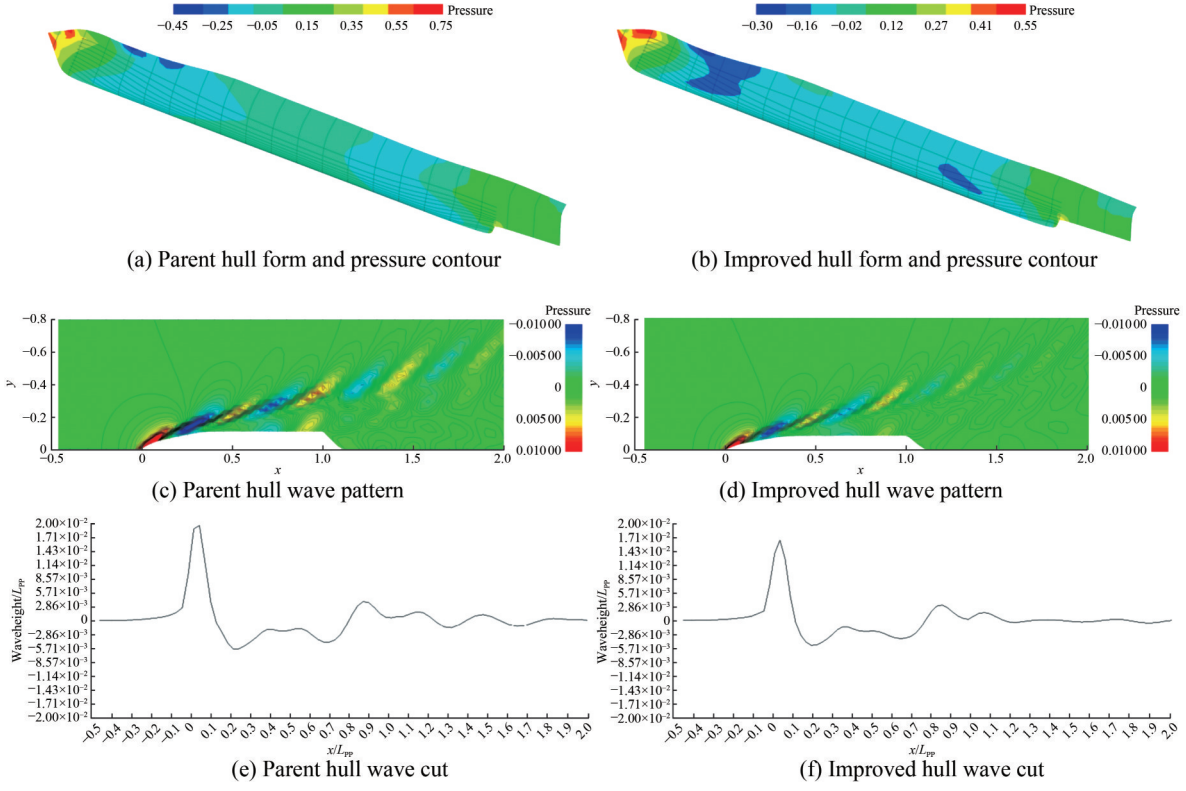
Table 13 Resistance coefficients for both the parent and improved hulls of MV Ferry Boat-1

Resistance coefficient	Parent hull	Improved hull	Change (%)
C_F	1.8×10^{-3}	1.805×10^{-3}	+0.99
C_{PV}	2.6×10^{-3}	2.2×10^{-3}	−13.29
C_V	4.4×10^{-3}	4×10^{-3}	−8.20
C_W	2.4×10^{-3}	2×10^{-3}	−18.38
C_T	6.8×10^{-3}	6×10^{-3}	−11.82

mon vertical axis of wave height/L_{BP}. The wave-cut diagrams shared the same scale, allowing direct comparison of crest/trough heights between the parent and improved hulls. Peak values are tabulated in Table 19.

4.3 Wave-pattern validation

The crest elevations of all wave-cut plots were derived from normalized free-surface data output by Shipflow and converted into dimensional units using each hull's length



(a) Parent hull form and pressure contour

(b) Improved hull form and pressure contour

(c) Parent hull wave pattern

(d) Improved hull wave pattern

(e) Parent hull wave cut

(f) Improved hull wave cut

Figure 7 Wave pattern and wave cut of MV Ferry Boat-1

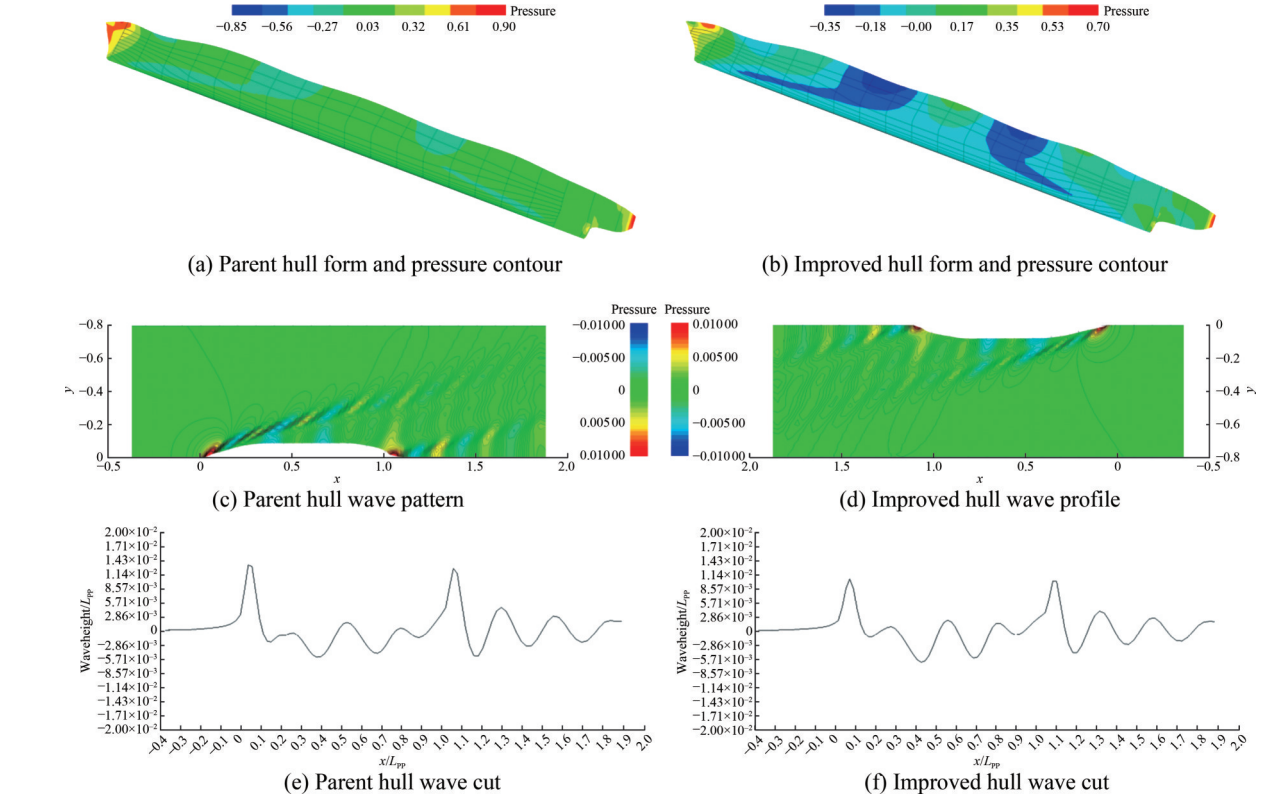
Table 14 Comparison between the parent and improved designs of MV Swapan

Design particulars	Parent design	Improved design	Change (%)	Qualitative recommendation	Quantitative recommendation ranges	Design recommendations addressed?
L_{WL}	43.76	45	2.83	Increase	–	Yes
B	7.77	7.3	−6.05	–	–	–
L_{WL}/B	5.63	6.16	9.41	Increase	3.74–6.21	Yes
T	1.6	1.82	0	–	–	–
B/T	3.39	4.01	34.51	Decrease	3.33–6.54	The B/T ratio is within the quantitative recommendation range. However, it had to increase to keep the same GT.
C_B	0.66	0.6	−9.09	Minimum C_B that meets capacity and stability requirements		Yes
F_N	0.24	0.23	−4.17	Decrease	0.23–0.32	Yes
GT	536	536	0	Increase	237–640	For fair comparison, GT was kept the same for both cases. Therefore, the qualitative recommendation was not met.
V_s	9.5	9.5	0	Decrease	9.00–12.00	For fair comparison, the speed was kept the same for both cases. Therefore, the qualitative recommendation was not met.

Table 15 Resistance coefficients for both the parent and improved hulls of MV Swapan

Resistance coefficient	Parent hull	Improved hull	Change (%)
C_F	1.93×10^{-3}	1.96×10^{-3}	1.97
C_{PV}	4.6×10^{-4}	4.6×10^{-4}	−0.30
C_V	2.39×10^{-3}	2.42×10^{-3}	1.59
C_W	6.3×10^{-4}	2.0×10^{-4}	−67.73
C_T	3.02×10^{-3}	2.63×10^{-3}	−12.98

between perpendiculars (L_{pp}). Table 19 presents the peak crest values for both parent and optimized hull forms. Across all six vessels, the optimized designs showed crest height reductions between 11% and 16%, aligning with the observed decrease in wave-making resistance. XPAN's solver is known to predict wave fields within ±5 mm accuracy for $F_N = 0.15 - 0.30$, further supporting the physical plausibility of the presented wave patterns.



(a) Parent hull form and pressure contour

(b) Improved hull form and pressure contour

(c) Parent hull wave pattern

(d) Improved hull wave profile

(e) Parent hull wave cut

(f) Improved hull wave cut

Figure 8 Wave pattern and wave cut of MV Swapan

Table 16 Comparison between the parent and improved designs of MV Running Sun

Design particulars	Parent design	Improved design	Change (%)	Qualitative recommendation	Quantitative recommendation ranges	Design recommendations addressed?
L_{WL}	34.15	35	2.49	Increase	–	Yes
B	6.77	5.65	−16.54	–	–	–
L_{WL}/B	5.04	6.19	22.91	Increase	3.74–6.21	Yes
T	1.35	1.69	25.19	–	–	–
B/T	5.015	3.34	−33.34	Decrease	3.33–6.54	Yes
C_B	0.65	0.607	−6.62	Minimum C_B that meets capacity and stability requirements		Yes
F_N	0.253	0.249	−1.58	Decrease	0.23–0.32	Yes
GT	209	209	0	Increase	237–640	For fair comparison, *GT* was kept the same for both cases. Therefore, the qualitative recommendation was not met.
V_s	9	9	0	Decrease	9.00–12.00	For fair comparison, the speed was kept the same for both cases. Therefore, the qualitative recommendation was not met.

Table 17 Resistance coefficients for both the parent and improved hulls of MV Running Sun

Resistance coefficient	Parent hull	Improved hull	Change (%)
C_F	1.990×10^{-3}	1.917×10^{-3}	−3.67
C_{PV}	5.190×10^{-4}	4.400×10^{-4}	−15.31
C_V	2.510×10^{-3}	2.357×10^{-3}	−6.10
C_W	2.133×10^{-3}	1.499×10^{-3}	−29.72
C_T	4.643×10^{-3}	3.855×10^{-3}	−16.97

4.4 Comparison of the hybrid and full RANS models for resistance prediction

To evaluate the hybrid model's suitability for viscous-dominated flows, we compared it with Shipflow's full RANS solver (XCHAP) across all 12 cases. The hybrid model combined XPAN (wave resistance), XBOUND (frictional resistance), and XCHAP (aft region), whereas the full RANS model used XCHAP for the entire flow field. Table 19 presents the frictional (C_F) and total (C_T) resistance coefficients. The full RANS model showed slightly lower C_F values, indicating better viscous effect capture, whereas the C_T trends aligned with the hybrid model. These support this study's resistance improvement findings.

4.5 Discussion

The CFD simulations in this study provide detailed hydrodynamic insights into resistance reductions achieved through hull optimizations for six inland vessels. These optimizations—adjusting waterline length-to-beam ratio (L_{WL}/B), block coefficient (C_B), and beam-to-draft ratio (B/T)—yielded total resistance reductions of 5.56%–17.27%, as detailed in Tables 7, 9, 11, 13, 15, and 17. This section analyzes the key hydrodynamic mechanisms behind these improvements, supported by wave-pattern visualizations (Figures 3–8), peak crest elevation data (Table 19), and resistance coefficient comparisons.

A key factor in these resistance reductions is the decrease in wave-making resistance (C_W), driven by a higher L_{WL}/B ratio, which results in a more slender hull. Per the Kelvin wave theory (Wang, 2003), slender hulls reduce wave interference and delay divergent wave formations, lowering wave-induced drag. This is evident in Figures 3–8, which show reduced wave heights for the optimized hulls, and Table 18, which reports 11%–16% reductions in peak wave crest elevations across all vessels. For example, MV Swapan exhibits a 67.73% reduction in C_W (Table 15), underscoring the effectiveness of increased waterline length in minimizing wave energy dissipation. This is particularly critical in inland waterways, where shallow water amplifies wave effects.

Stern flow optimization significantly reduces viscous pressure resistance (C_{PV}). CFD results indicate improved local pressure recovery near the stern, lowering C_{PV} by up to 19.10% (e.g., OT Moina; Table 11). This stems from refined aftbody designs that minimize flow separation and wake turbulence. Velocity streamline plots show smoother stern flow in optimized hulls, reducing vortex shedding and pressure drag and thus enhancing propulsive efficiency. The wave patterns in Figures 3–8 further confirm lower pressure gradients at the stern, aligning with the observed C_{PV} reductions. These findings emphasize the value of aftbody refinements for inland ships operating in confined channels.

Adjustments to the B/T ratio optimize wetted surface distribution, influencing the frictional resistance (C_F). Although the increased draft slightly raises the wetted surface area, it promotes a smoother boundary-layer transi-

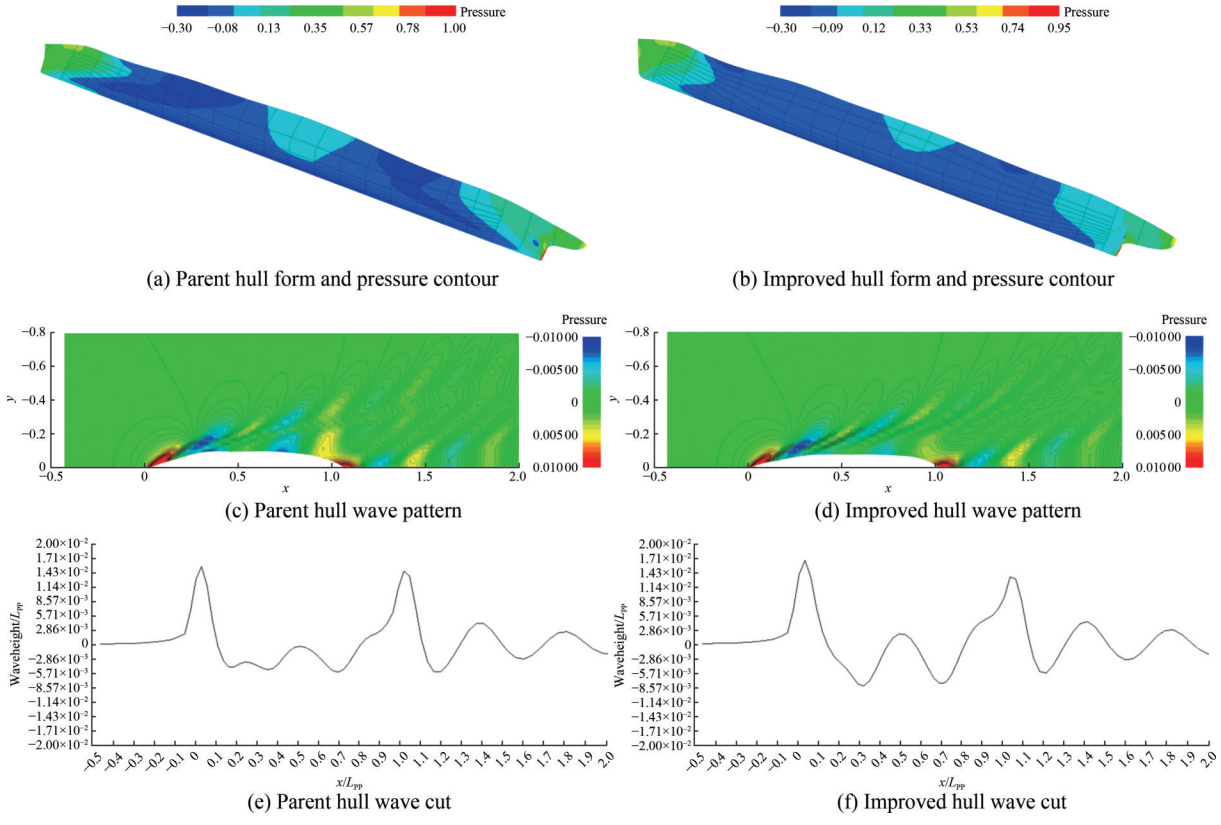


Figure 9 Wave pattern and wave cut of MV Running Sun

Table 18 Peak free-surface crest elevations for parent vs. improved hulls (F_N range of 0.17–0.26)

Vessel	Parent (m)	Improved (m)	ΔCrest (%)
OT-1049	0.0408	0.0360	–11.76
OT-Zarifa	0.0380	0.0331	–12.89
OT-Moina	0.0330	0.0291	–11.82
MV ferry Boat-1	0.0378	0.0319	–15.61
MV swapan	0.0380	0.0320	–15.79
MV running sun	0.0440	0.0383	–12.95

Table 19 Comparison of resistance coefficients from the hybrid and full RANS models ($\times 10^{-3}$)

Vessel	Hybrid C_F	Full RANS C_F	Hybrid C_T	Full RANS C_T
OT 1049	1.68	1.65	4.06	4.05
OT zarifa	1.84	1.80	4.04	4.02
OT moina	1.64	1.62	2.93	2.92
MV ferry Boat-1	1.80	1.78	6.80	6.78
MV swapan	1.93	1.90	3.02	3.01
MV running Sun	1.99	1.96	4.64	4.62

tion, delaying turbulence onset. This results in lower shear stress, with C_F reductions of up to 7.06% (e.g., OT Zarifa; Table 9). CFD simulations reveal that optimized hulls maintain laminar flow further along the hull, reducing frictional drag—a key consideration in shallow-water environments, where boundary-layer dynamics are pronounced.

Figure 9 visually summarizes the findings with a bar chart comparing the frictional (C_F), viscous pressure (C_{PV}), wave (C_W), and total (C_T) resistance coefficients for the parent and optimized hulls across all six vessels. The chart highlights consistent C_T reductions (5.56%–17.27%), driven by decreases in C_W (up to 67.73%), C_{PV} (up to 19.10%), and C_F (up to 7.06%), validating the effectiveness of the proposed optimizations. The sensitivity analysis using the Holtrop–Mennen method (Table 4) complements these insights by showing how design parameter changes (e.g., 5% increase in L_{WL}) affect resistance trends, although its limitations in shallow water are noted in Section 4.

Although these CFD insights elucidate hydrodynamic mechanisms, additional visualizations–such as velocity vector diagrams and hull surface shear–stress distributions–can further clarify flow behaviors in confined waterways. Experimental validation via towing tank tests, as proposed in Section 5, can also strengthen these findings and support practical implementation.

The optimized hull designs yield preliminary fuel savings of 4%–15% (Section 4.2), reflecting reduced power requirements. These savings, combined with the obtained hydrodynamic insights, highlight the potential of CFD-based optimization in enhancing the efficiency and sustain-

ability of inland ships in Bangladesh's navigational environment. Future studies should explore additional design parameters and operational conditions to further refine these optimizations.

5 Conclusions

This research successfully demonstrated the effectiveness of the proposed design improvement methods for inland oil tankers and passenger ships in Bangladesh. With the use of advanced CFD simulations, significant reductions in hydrodynamic resistance were observed for all the test ships, proving the proposed design modifications' energy efficiency while maintaining operational stability.

Although the results were favorable, limitations encountered during the application of some of the design recommendations should be pointed out, particularly for vessels operating in shallow draft conditions. For instance, for MV Swapan, all qualitative design changes could not be achieved due to limitations in the draft. Nevertheless, significant resistance reduction was still achieved. These operating restrictions highlight the necessity of specially designed solutions accounting for specific navigational conditions of inland waterways. The application of CFD simulations during this study enabled a deep analysis of fluid–structure interaction with high cost-effectiveness, instead of costly physical model experiments. However, as in any numerical method, there are physical limitations, primarily the accurate prediction of flow separation and drag coefficients. Follow-up studies should comprise towing tank trials and sea trials to experimentally validate CFD predictions. These experiments can enhance the validity of the results and ensure that the design improvements translate to actual benefits in ship operation. Furthermore, the broader implications of the design improvements are not only hydrodynamic resistance. Decreasing resistance leads to less fuel consumption, lower GHG emissions, and economic benefits to operators. If vessel designs are optimized, Bangladesh's inland waterway transport network can transform its operations into a more energy-efficient and greener transport network consistent with international visions, such as the International Maritime Organization's schemes for reducing maritime emissions.

The design guidelines proposed in this study can serve as the basis for a scalable optimization framework targeting the broader inland fleet of Bangladesh. Given that more than 10 000 inland cargo and tanker vessels operate in Bangladesh's waterways, the adoption of hydrodynamically optimized hull designs can yield significant national-level reductions in fuel consumption and GHG emissions. To facilitate this transition, collaboration between shipbuilders, regulators (e. g., BIWTA), and private operators is essential.

Additionally, the integration of this optimization approach with policy instruments, such as green financing, energy-efficiency subsidies, or carbon credit schemes (e. g., under a national GHG inventory or monitoring, reporting, and verification system), can incentivize adoption. The results presented here can inform evidence-based standards for inland vessel design and retrofitting under sustainability frameworks. Future work should explore the institutional and economic mechanisms needed to implement this framework on a fleet-wide scale, including pilot programs and incentive models.

Nomenclature

L_{WL}	Water line length (m)
L_{WL}/B	Length/breadth
B/T	Breadth/draft
DWT/∇	Dead weight/displacement
C_B	Block coefficient
V_s	Ship speed (Knot)
F_N	Froude number
GT	Gross tonnage
C_F	Frictional resistance coefficient
C_{PV}	Viscous pressure resistance coefficient
C_V	Viscous resistance coefficient
C_W	Wave-resistance coefficient
C_T	Total resistance coefficient

Acknowledgement The authors acknowledge the Bangladesh University of Engineering and Technology (BUET) for all its support in doing this research.

Competing interests The authors have no competing interests to declare that are relevant to the content of this article.

References

Bappy MMH, Hasan SMR (2024) Enhancing inland vessel efficiency: A comprehensive study on the effectiveness of bulbous bow in mitigating resistance in Bangladesh. Results in Engineering 24: 103394. https://doi.org/10.1016/j.rineng.2024.103394

BIWTA (2023) Communication strategy and plan. Bangladesh Inland Water Transport Authority (BIWTA), Dhaka, Bangladesh, IDA Credit No. 5842-BD, Contract No. BRWTP-S16

Boussinesq J (1878) Supplement to "The Collection of Essays on Water Flow Theory". Journal of Pure and Applied Mathematics 4: 335-376. (in French) http://www.numdam.org/item?id=JMPA_1878_3_4__335_0

Celik IB, Ghia U, Roache PJ, Freitas CJ (2007) Procedure for estimation and reporting of uncertainty due to discretization in CFD applications. Journal of Fluids Engineering 130(7): 078001.

https://doi.org/10.1115/1.2960953

Cheng Y, Sayde C, Li Q, Basara J, Selker J, Tanner E, Gentine P (2017) Failure of Taylor's hypothesis in the atmospheric surface layer and its correction for eddy-covariance measurements. Geophysical Research Letters 44(9): 4287-4295. https://doi.org/10.1002/2017GL073499

Courant R, Friedrichs K, Lewy H (1967) On partial difference equations of mathematical physics. IBM Journal 11: 215-234. (in Germany)

Dowding K, Sandia National Laboratories (2016) Overview of ASME V&V 20-2009 standard for verification and validation in computational fluid mechanics and heat transfer. Virginia Military Institute, Inverse Problems Symposium, Sandia Corporation, Lockheed Martin Company, United States Department of Energy, & National Nuclear Security Administration. https://www.osti.gov/servlets/purl/1368927

Du P, Ouahsine A, Sergent P, Hu H (2020) Resistance and wave characterizations of inland vessels in the fully-confined waterway. Ocean Engineering 210: 107580. https://doi.org/10.1016/j.oceaneng.2020.107580

Eliasson S, Olsson D (2011) Barge stern optimization analysis on a straight shaped stern using CFD. Master thesis, Chalmers University of Technology, Gothenburg, Sweden, 7-9

Hasan SMR, Karim MM (2020) Proposed inland oil tanker design in Bangladesh focusing CO_2 emission reduction based on revised EEDI parameters. Journal of Marine Science and Engineering 8(9): 658. https://doi.org/10.3390/jmse8090658

Hasan SMR, Karim MM (2022) Energy efficiency design index baselines for ships of Bangladesh based on verified ship data. Heliyon 8(10): e10996. https://doi.org/10.1016/j.heliyon.2022.e10996

Hasan SMR, Karim MM (2023) Energy-efficient inland cargo ship design based on fuel consumption and CO_2 emission control using CFD. Journal of Naval Architecture and Marine Engineering 20(3): 1-10. https://doi.org/10.3329/jname.v20i3.63664

Holtrop J, Mennen GGJ (1982) An approximate power prediction method. International Shipbuilding Progress 29(335): 166-170

Larsson L, Raven HC (2010) Ship resistance and flow. The Principles of Naval Architecture Series, The Society of Naval Architects and Marine Engineers, New York

Nabila N (2014) Numerical simulation of flow around ship hull considering rudder-propeller interaction. Master thesis, Bangladesh University of Engineering and Technology, Dhaka, Bangladesh, 11-32

Natalia CR, Inga B, Fabio B (2024) Barriers and solutions for sustainable development of inland waterway transport: A literature review. Transport Economics and Management 2: 31-44. https://doi.org/10.1016/j.team.2024.01.001

Onwuegbuchunam DE, Ogbenna FC, Ezeanya NC, Okeke KO (2019) Ship hull form optimization: A computational fluid dynamics (CFD) approach. International Journal of Transportation Engineering and Technology 5(3): 43. https://doi.org/10.11648/j.ijtet.20190503.11

Orych M, Werner S, Larsson L (2021) Validation of full-scale delivered power CFD simulations. Ocean Engineering 238: 109654. https://doi.org/10.1016/j.oceaneng.2021.109654

Prandtl L (1904) Motion of fluids with very little viscosity. National Advisory Committee for Aeronautics, Washington, Technical Memorandum No. 452

Rørdam OH, Winther M, Ellermann T, Christensen J, Marlene P (2009) Ship emissions and air pollution in Denmark. National Environmental Research Institute Aarhus University, Aarhus, Denmark, Environmental Project No. 1307 2009

Uddin MI, Islam MR, Awal ZI, Newaz KMS (2017) An analysis of accidents in the inland waterways of Bangladesh: Lessons from a decade (2005-2015). Procedia Engineering 194: 291-297. https://doi.org/10.1016/j.proeng.2017.08.148

Wang B (2003) Kelvin waves. Encyclopedia of Atmospheric Sciences, 1062-1068. https://doi.org/10.1016/b0-12-227090-8/00191-3